

# Reflection and transmission coefficients of a fracture in transversely isotropic media

JOSÉ M. CARCIONE AND STEFANO PICOTTI

Istituto Nazionale di Oceanografia e di Geofisica Sperimentale (OGS), Borgo Grotta Gigante 42c,  
34010 Sgonico, Trieste, Italy (jcarcione@inogs.it)

Received: June 17, 2011; Revised: September 7, 2011; Accepted: September 19, 2011

---

## ABSTRACT

We obtain the reflection and transmission coefficients at a fracture in transversely isotropic media, whose symmetry axis is perpendicular to the fracture surface. We consider dissimilar upper and lower media. The fracture is modeled as an interface with boundary discontinuities in the displacement and the particle velocity. The stress components are proportional to the displacement and velocity discontinuities through the specific stiffnesses and specific viscosities, respectively. The stiffness introduces frequency-dependence and phase changes in the fracture response and the viscosity is related to the energy loss. We also calculate the energy balance at the fracture and the dissipated energy. The theory is illustrated by computing the reflection coefficient of a fracture present in the Antarctic ice cap. In this case, the reflection coefficient decreases with increasing incidence angle and then approaches 1 at grazing angle.

Keywords: fracture, anisotropy, reflection coefficient, boundary condition, attenuation

## 1. INTRODUCTION

The study of the reflection-transmission problem of a fracture plays an important role in seismology, exploration geophysics and material science: fractures and cracks in the Earth's crust may constitute possible sources of earthquakes (Pyrak-Nolte *et al.*, 1990), and hydrocarbon and geothermal reservoirs are mainly composed of fractured rocks (Nakagawa and Myer, 2009). Moreover, ultrasonic waves are used to detect flaws and cracks in order to prevent material failure (Nagy and Adler, 1990). Applications in geotechnical engineering, such as the analysis of dynamic stability of rock slopes and tunnels, involve the study of imperfect joints in rock masses (Perino *et al.*, 2010; Fan *et al.*, 2011). In geophysical prospecting, knowledge of reservoirs fracture orientations, densities and sizes is essential, since these factors control hydrocarbon production (Hansen, 2002; Hall and Kendall, 2003; Grechka and Tsvankin, 2003; Barton, 2007).

The simulation of a fracture requires a suitable interface model for describing its dynamic response. Theories that consider imperfect contact were mainly based on the displacement discontinuity model at the interface. Pyrak-Nolte *et al.* (1990) proposed a non-welded interface model based on the discontinuity of the displacement and the

particle velocity across the interface. The stress components are proportional to the displacement and velocity discontinuities through the specific stiffnesses and one specific viscosity, respectively. Displacement discontinuities conserve energy and yield frequency dependent reflection and transmission coefficients. On the other hand, velocity discontinuities generate an energy loss at the interface. The specific viscosity accounts for the presence of a liquid under saturated conditions. The liquid introduces a viscous coupling between the two surfaces of the fracture (*Schoenberg, 1980*) and enhances energy transmission, but at the same time this is reduced by viscous losses. The model may account for some slip and dilatancy effects as those described, for instance, by the interface model proposed by *Mroz and Giambianco (1996)*. *Coates and Schoenberg (1995)* implement Schoenberg's linear-slip model in finite-difference simulations, while an approach to explicitly simulate cracks and fractures is proposed by *Zhang and Gao (2009)*.

The reflection-transmission problem in isotropic media has been solved by *Carcione (1996, 2007)* and *Carcione (1998)* obtained the normal-incidence reflection and transmission coefficients of a fracture embedded in a homogeneous transversely isotropic (TI) medium. In both cases, numerical simulations were performed by using a pseudospectral method. Elastic-wave scattering by a circular crack in a TI solid was investigated by *Kundu and Boström (1992)*. They used an analytical solution method and considered stress-free boundary conditions at the fracture interface, implying a complete decoupling of the two surfaces which corresponds to zero stiffnesses and zero specific viscosity. *Chaisri and Krebes (2000)* obtained the same expressions of *Carcione (1996)* in the particular case of no energy loss.

In this work, we obtain the reflection and transmission coefficients for all phase and ray angles of incidence by considering displacement and particle-velocity discontinuities at the interface of the fracture embedded in a TI medium. The consideration of a TI medium is the novelty of the present work and generalizes the previous theory mentioned above. The imperfect bonding is described by four parameters: the normal and tangential specific stiffnesses and viscosities. In order to model a fracture embedded in a finely laminated medium, we assume that this is described by a TI medium whose symmetry axis is perpendicular to the fracture surface. For instance, composite materials, or geological layers whose stratification plane is parallel to the Earth's surface. The equivalence between a laminated medium and a TI medium holds when the dominant wavelength of the signal is long compared to the thickness of the layers (*Backus, 1962; Carcione, 2007*). Moreover, we obtain the energy balance, giving the energy reflection-transmission coefficients and the energy dissipated due to the fracture specific viscosities.

## 2. INTERFACE MODEL AND STRESS-STRAIN RELATIONS

Let us consider a planar fracture separating two elastic TI media. The non-ideal characteristics of the fracture are modeled through the boundary conditions. The model proposed here is based on the discontinuity of the displacement and particle-velocity fields across the fracture interface. We consider the  $(x, z)$ -plane, and refer to the upper and lower media with the labels 1 and 2, respectively, with  $z$  increasing towards the lower

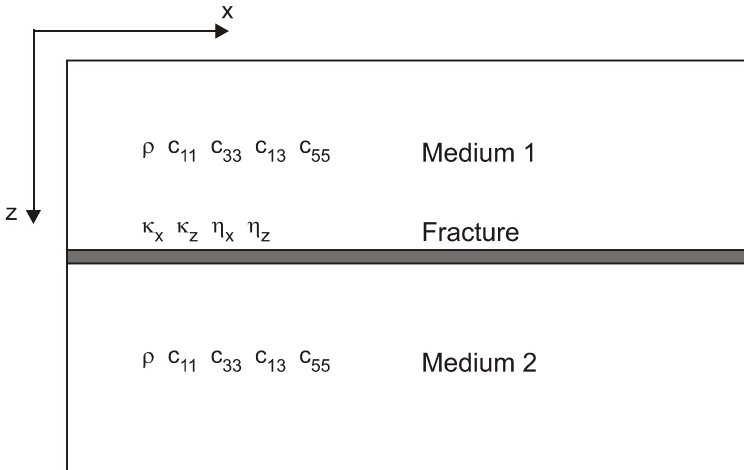


**Fig. 1.** Planar fracture embedded in transversely isotropic media of dissimilar density and elastic constants.

medium (see Fig. 1). Then, the boundary conditions for a wave impinging on the fracture ( $z = 0$ ) are (Carcione, 1998)

$$\begin{aligned} \kappa_x [u_x] + \eta_x [v_x] &= \sigma_{xz}, \\ \kappa_z [u_z] + \eta_z [v_z] &= \sigma_{zz}, \\ [\sigma_{xz}] &= 0, \\ [\sigma_{zz}] &= 0, \end{aligned} \quad (1)$$

where  $u_x$  and  $u_z$  are the displacement components,  $v_x$  and  $v_z$  are the particle-velocity components,  $\sigma_{xz}$  and  $\sigma_{zz}$  are the stress components,  $\kappa_x$  and  $\kappa_z$  are specific stiffnesses and  $\eta_x$  and  $\eta_z$  are specific viscosities. They have dimensions of stiffness and viscosity per unit length, respectively. Moreover, the brackets denote discontinuities across the fracture interface, such that for a field variable  $\phi$ , it is  $[\phi] = \phi_2 - \phi_1$ .

The model simulates the fracture by a zero width layer of distributed spring-dashpots. It can be shown that relaxation-like functions of Maxwell or Kelvin-Voigt type govern the tangential and normal coupling properties of the crack. The fracture exhibits time dependent mechanical properties through the relaxation functions, and, as in a viscoelastic material, this implies energy dissipation. A displacement discontinuity ( $\kappa_z \neq 0$ ) yields a change of phase, while a discontinuity in the particle velocity ( $\eta_z \neq 0$ ) implies an energy loss at the fracture (Carcione, 1996, 1998, 2007);  $\kappa_i = 0$ ,  $i = 1(x), 3(z)$  gives the particle-velocity discontinuity model and  $\eta_i = 0$  gives the displacement discontinuity model. On the other hand, if  $\eta_i \rightarrow \infty$  or  $\kappa_i \rightarrow \infty$ , the model gives the welded interface.

The characteristics of the medium are completed with the constitutive relations (*Aki and Richards, 1980; Carcione, 2007*)

$$\begin{aligned}\sigma_{xx} &= c_{11}\partial_x u_x + c_{13}\partial_z u_z, \\ \sigma_{zz} &= c_{13}\partial_x u_x + c_{33}\partial_z u_z, \\ \sigma_{xz} &= c_{55}(\partial_x u_z + \partial_z u_x),\end{aligned}\quad (2)$$

where  $c_{IJ}$  are the elastic constants of the medium and  $\partial_i$  indicates partial derivative with respect to the spatial variable  $x_i$ .

### 3. PROPAGATION CHARACTERISTICS IN THE TI MEDIUM

A general plane-wave solution for the displacement field  $\mathbf{u} = (u_x, u_z)$

$$\mathbf{u} = \mathbf{U} \exp[i\omega(t - s_x x - s_z z)], \quad (3)$$

where  $s_x$  and  $s_z$  are the components of the slowness vector,  $\mathbf{U}$  is a complex vector,  $t$  is the time variable,  $\omega$  is the angular frequency and  $i = \sqrt{-1}$ .

The dispersion relation of a TI medium is (e.g., *Carcione, 2007*)

$$(c_{11}s_x^2 + c_{55}s_z^2 - \rho)(c_{33}s_z^2 + c_{55}s_x^2 - \rho) - (c_{13} + c_{55})^2 s_x^2 s_z^2 = 0, \quad (4)$$

where  $\rho$  is the mass density. Eq.(4) has two solutions corresponding to the quasi-compressional (P) and quasi-shear (S) waves.

In order to distinguish between down and up propagating waves, the slowness relation equation (4) is solved for  $s_z$ , given the horizontal slowness  $s_x$ . This yields

$$s_z = \pm \frac{1}{\sqrt{2}} \sqrt{K_1 \mp \text{pv} \sqrt{K_1^2 - 4K_2 K_3}} \quad (5)$$

where

$$\begin{aligned}K_1 &= \rho \left( \frac{1}{c_{55}} + \frac{1}{c_{33}} \right) + \frac{1}{c_{55}} \left[ \frac{c_{13}}{c_{33}} (c_{13} + 2c_{55}) - c_{11} \right] s_x^2, \\ K_2 &= \frac{1}{c_{33}} (c_{11}s_x^2 - \rho), \quad K_3 = s_x^2 - \frac{\rho}{c_{55}},\end{aligned}$$

and “pv” denotes the principal value. The signs in  $s_z$  correspond to

- (+,-) downward propagating P wave,
- (+,+) downward propagating S wave,
- (-,-) upward propagating P wave,
- (-,+)

upward propagating S wave.

The plane-wave eigenvectors (polarizations) belonging to a particular eigenvalue can be obtained from the P-S Kelvin-Christoffel equation (*Carcione, 2007, Eq.(1.81)*). We obtain

$$\mathbf{U} = U_0 \begin{pmatrix} \beta \\ \xi \end{pmatrix}, \quad (6)$$

where  $U_0$  is the plane-wave amplitude and

$$\begin{aligned} \beta &= \text{pv} \sqrt{\frac{c_{55}s_x^2 + c_{33}s_z^2 - \rho}{c_{11}s_x^2 + c_{33}s_z^2 + c_{55}(s_x^2 + s_z^2) - 2\rho}}, \\ \xi &= \pm \text{pv} \sqrt{\frac{c_{11}s_x^2 + c_{55}s_z^2 - \rho}{c_{11}s_x^2 + c_{33}s_z^2 + c_{55}(s_x^2 + s_z^2) - 2\rho}}, \end{aligned} \quad (7)$$

where the + and – signs correspond to the P and S waves, respectively. From Eqs.(3) and (7), the particle-velocity field can be written as

$$\mathbf{v} = i\omega \mathbf{u} = i\omega U_0 \begin{pmatrix} \beta \\ \xi \end{pmatrix} \exp[i\omega(t - s_x x) - s_z z]. \quad (8)$$

Substituting the plane wave (8) into the stress-strain relation (2) yields

$$\sigma_{xx} = X, \quad \sigma_{zz} = Z \quad \text{and} \quad \sigma_{xz} = W, \quad (9)$$

where

$$\begin{aligned} X &= -i\omega U_0 (\beta c_{11}s_x + \xi c_{13}s_z), \\ Z &= -i\omega U_0 (\beta c_{13}s_x + \xi c_{33}s_z), \\ W &= -i\omega U_0 c_{55} (\xi s_x + \beta s_z). \end{aligned} \quad (10)$$

The slowness components are given by

$$s_x = \frac{\sin \theta}{v(\theta)}, \quad s_z = \frac{\cos \theta}{v(\theta)}, \quad (11)$$

where  $\theta$  is the phase propagation angle, measured with respect to the  $z$ -axis, and

$$v = \frac{1}{s} = \frac{1}{\sqrt{s_x^2 + s_z^2}} \quad (12)$$

is the phase velocity that can be obtained from the dispersion relation (4). Hence, we have

$$\rho v^2 = \frac{1}{2} \left( c_{55} + c_{11} \sin^2 \theta + c_{33} \cos^2 \theta \pm C \right), \quad (13)$$

with

$$C = \sqrt{\left[ (c_{33} - c_{55}) \cos^2 \theta - (c_{11} - c_{55}) \sin^2 \theta \right]^2 + (c_{13} + c_{55})^2 \sin^2 2\theta}. \quad (14)$$

The + sign corresponds to the P wave, and the – sign to the S wave.

#### 4. REFLECTION AND TRANSMISSION COEFFICIENTS

For clarity, the symbols  $P$  and  $S$  indicate the P and S waves, respectively. Moreover, the subscripts  $I$ ,  $R$  and  $T$  denote the incident, reflected and transmitted waves. Using symmetry properties to define the polarization of the reflected waves, the displacements for a P wave incident from above the fracture are given by

$$\mathbf{u}_1 = \mathbf{u}_{P_I} + \mathbf{u}_{P_R} + \mathbf{u}_{S_R}, \quad (15)$$

$$\mathbf{u}_2 = \mathbf{u}_{P_T} + \mathbf{u}_{S_T}, \quad (16)$$

where

$$\mathbf{u}_{P_I} = (\beta_{P_1}, \xi_{P_1}) \exp[i\omega(t - s_x x - s_z P_1 z)], \quad (17)$$

$$\mathbf{u}_{P_R} = R_{PP} (\beta_{P_1}, -\xi_{P_1}) \exp[i\omega(t - s_x x + s_z P_1 z)], \quad (18)$$

$$\mathbf{u}_{S_R} = R_{PS} (\beta_{S_1}, -\xi_{S_1}) \exp[i\omega(t - s_x x + s_z S_1 z)], \quad (19)$$

$$\mathbf{u}_{P_T} = T_{PP} (\beta_{P_2}, \xi_{P_2}) \exp[i\omega(t - s_x x - s_z P_2 z)], \quad (20)$$

$$\mathbf{u}_{S_T} = T_{PS} (\beta_{S_2}, \xi_{S_2}) \exp[i\omega(t - s_x x - s_z S_2 z)]. \quad (21)$$

Application of Snell's law implies the continuity of the horizontal slowness  $s_x$ . The boundary conditions do not influence the emergence angles of the transmitted and reflected waves. The vertical slownesses  $s_z P$  and  $s_z S$ , as well as  $\beta_P$ ,  $\beta_S$ ,  $\xi_P$  and  $\xi_S$ , follow respectively the  $(+, -)$  and  $(+, +)$  sign sets given in Eq.(5). The choice  $U_0 = 1$  implies no loss of generality.

The boundary conditions (1) are

$$[u_x] = c_x \sigma_{xz}, \quad [u_z] = c_z \sigma_{zz}, \quad [\sigma_{xz}] = 0, \quad [\sigma_{zz}] = 0, \quad (22)$$

and

$$c_i = \frac{1}{\kappa_i + i\omega\eta_i}, \quad i = 1(x), 3(z) \quad (23)$$

is a complex compliance per unit length characterizing the fracture.

Using the equations for the displacements and stresses, the boundary conditions generate the following matrix equation for the reflection and transmission coefficients:

$$\begin{pmatrix} \beta_{P_1} - c_x W_{P_1} & \beta_{S_1} - c_x W_{S_1} & -\beta_{P_2} & -\beta_{S_2} \\ \xi_{P_1} - c_z Z_{P_1} & \xi_{S_1} - c_z Z_{S_1} & \xi_{P_2} & \xi_{S_2} \\ Z_{P_1} & Z_{S_1} & -Z_{P_2} & -Z_{S_2} \\ W_{P_1} & W_{S_1} & W_{P_2} & W_{S_2} \end{pmatrix} \begin{pmatrix} R_{PP} \\ R_{PS} \\ T_{PP} \\ T_{PS} \end{pmatrix} = \begin{pmatrix} -\beta_{P_1} - c_x W_{P_1} \\ \xi_{P_1} + c_z Z_{P_1} \\ -Z_{P_1} \\ W_{P_1} \end{pmatrix}, \quad (24)$$

where  $W$  and  $Z$  are given by Eqs.(10).

The steps to compute the reflection and transmission coefficients are the following:

1. The horizontal slowness  $s_x$  is the independent parameter. It is the same for all the waves (Snell's law). For an incident wave, the independent variable becomes the incidence angle  $\theta$ , and  $s_x$  is obtained from Eq.(11).
2. Compute  $s_{zP_1}$ ,  $s_{zS_1}$ ,  $s_{zP_2}$  and  $s_{zS_2}$  from Eq.(5), where the first sign is positive. For an incident wave,  $s_{zP_1}$  can be calculated either from Eq.(5) or from Eq.(11).
3. Compute  $\beta_{P_1}$ ,  $\beta_{S_1}$ ,  $\beta_{P_2}$ ,  $\beta_{S_2}$ ,  $\xi_{P_1}$ ,  $\xi_{S_1}$ ,  $\xi_{P_2}$  and  $\xi_{S_2}$  from Eqs.(7).
4. Compute  $W_{P_1}$ ,  $W_{S_1}$ ,  $W_{P_2}$  and  $W_{S_2}$  and  $Z_{P_1}$ ,  $Z_{S_1}$ ,  $Z_{P_2}$  and  $Z_{S_2}$  from Eqs.(10).
5. Compute the reflection and transmission coefficients by numerically solving Eq.(24).

Eq.(24) gives the results of *Carcione (1996)* in the isotropic case, i.e., if  $c_{33} = c_{11}$  and  $c_{13} = c_{11} - 2c_{55}$ . *Carcione (1996)* obtained the potential amplitude coefficients, which are related to the displacement amplitude coefficients by a conversion factor. In the case of isotropy and similar upper and lower media, the conversion factor from one type of coefficient to the other is 1 for PP coefficients and  $v_S/v_P$  for PS coefficients, where  $v_P$  and  $v_S$  denote the P- and S-wave velocities (*Aki and Richards, 1980, p. 139*).

When  $c_x = c_z = 0$ , Eq.(24) yield the reflection and transmission coefficients of a welded interface as in *Wright (1987)*. At normal incidence and similar upper and lower media, we obtain (*Carcione, 1998*)

$$R_{PP} = \left( i \frac{\omega_P}{\omega} - \frac{2\eta_z}{I_P} - 1 \right)^{-1} = \left( \frac{2i}{\omega I_P c_z} - 1 \right)^{-1} \quad (25)$$

and

$$T_{PP} = 1 + R_{PP}, \quad (26)$$

where  $I_P = \sqrt{\rho c_{33}}$  and  $\omega_P = 2\kappa_z/I_P$  is the characteristic frequency that defines the transition from an apparently perfect interface to the apparently decoupled one. If  $\kappa_z = 0$ , it is  $\omega_P = 0$  and the particle-velocity discontinuity model is obtained. In this case, the coefficients are frequency independent and there are no phase changes. On the other hand, when  $\eta_z = 0$ , the theory gives the displacement discontinuity model. A discontinuity in the particle velocity implies energy dissipation at the fracture (*Carcione, 1996, 1998*). Moreover, if  $\eta_z \rightarrow 0$  and  $\kappa_z \rightarrow 0$ ,  $R_{PP} \rightarrow 1$  and  $T_{PP} \rightarrow 0$ , and the free surface condition is obtained; when  $\eta_z \rightarrow \infty$  or  $\kappa_z \rightarrow \infty$ ,  $R_{PP} \rightarrow 0$  and  $T_{PP} \rightarrow 1$ , giving the solution for a welded contact.

The coefficients are shown here as a function of the incidence ray angle  $\psi$ , which defines the direction of the energy-flux vector of the incidence wave. The ray angle can be obtained as (*Carcione, 2007*)

$$\tan \psi = \frac{\operatorname{Re}(\beta_{P_1}^* X_{P_1} + \xi_{P_1}^* W_{P_1})}{\operatorname{Re}(\beta_{P_1}^* W_{P_1} + \xi_{P_1}^* Z_{P_1})}, \quad (27)$$

where “Re” takes real part and “\*” denotes complex conjugate. Eq.(27) holds for an incident viscoelastic medium. In this work, the medium is elastic and the real part and complex conjugate operation can be removed.

## 5. ENERGY BALANCE AND LOSS

In a completely welded interface, the normal component of the time-averaged energy flux is continuous across the plane separating the two media. This is a consequence of the boundary conditions that impose continuity of normal stress and particle velocity. The same property is valid if  $\eta_x = \eta_z = 0$  (Carcione, 1996; Chaisri and Krebes, 2000). If the viscosities are non-zero, there is energy dissipation as shown in the following. Since the media are elastic, the interference fluxes between different waves vanish and only the fluxes corresponding to each single beam need be considered (Carcione, 2007). Denoting by  $F$  the vertical component of the energy flux, we have (Carcione, 2007)

$$\begin{aligned} -2F_{P_I} &= \operatorname{Re}(\sigma_{xzP_I} v_{xP_I}^* + \sigma_{zzP_I} v_{zP_I}^*), \\ -2F_{P_R} &= \operatorname{Re}(\sigma_{xzP_R} v_{xP_R}^* + \sigma_{zzP_R} v_{zP_R}^*), \\ -2F_{S_R} &= \operatorname{Re}(\sigma_{xzS_R} v_{xS_R}^* + \sigma_{zzS_R} v_{zS_R}^*), \\ -2F_{P_T} &= \operatorname{Re}(\sigma_{xzP_T} v_{xP_T}^* + \sigma_{zzP_T} v_{zP_T}^*), \\ -2F_{S_T} &= \operatorname{Re}(\sigma_{xzS_T} v_{xS_T}^* + \sigma_{zzS_T} v_{zS_T}^*). \end{aligned} \quad (28)$$

As shown by Carcione (1997, 2007), further algebra implies that the fluxes given in the preceding equations are proportional to the real parts of

$$\begin{aligned} F_{P_I} &\propto \beta_{P_1}^* W_{P_1} + \xi_{P_1}^* Z_{P_1}, \\ F_{P_R} &\propto -(\beta_{P_1}^* W_{P_1} + \xi_{P_1}^* Z_{P_1}) |R_{PP}|^2, \\ F_{S_R} &\propto -(\beta_{S_1}^* W_{S_1} + \xi_{S_1}^* Z_{S_1}) |R_{PS}|^2, \\ F_{P_T} &\propto (\beta_{P_2}^* W_{P_2} + \xi_{P_2}^* Z_{P_2}) |T_{PP}|^2, \\ F_{S_T} &\propto (\beta_{S_2}^* W_{S_2} + \xi_{S_2}^* Z_{S_2}) |T_{PS}|^2, \end{aligned} \quad (29)$$

where the proportionality factor is  $\frac{i}{2}\omega$ . We define the energy reflection and transmission coefficients as

$$ER_{PP} = \sqrt{\frac{F_{P_R}}{F_{P_I}}}, \quad ER_{PS} = \sqrt{\frac{F_{S_R}}{F_{P_I}}}, \quad ET_{PP} = \sqrt{\frac{F_{P_T}}{F_{P_I}}}, \quad ET_{PS} = \sqrt{\frac{F_{S_T}}{F_{P_I}}}. \quad (30)$$

The energy loss at the fracture is obtained by subtracting the energies of the reflected and transmitted waves from the energy of the incident wave. The normalized dissipated energy is

$$E_{loss} = 1 - ER_{PP}^2 - ER_{PS}^2 - ET_{PP}^2 - ET_{PS}^2. \quad (31)$$

At normal incidence we have

$$E_{loss} = 1 - |R_{PP}|^2 - |T_{PP}|^2. \quad (32)$$

Substituting Eqs.(25) and (26), the energy loss becomes

$$E_{loss} = \frac{\frac{4\eta_z}{I_P}}{\left(1 + \frac{2\eta_z}{I_P}\right)^2 + \left(\frac{\omega_P}{\omega}\right)^2}. \quad (33)$$

The maximum loss is obtained for

$$\eta_z = \frac{I_P}{2} \sqrt{1 + \left(\frac{\omega_P}{\omega}\right)^2}. \quad (34)$$

## 6. EXAMPLE

Seismic observations made in the vicinity of Dome C in East Antarctica show that the ice sheet there is TI with a vertical axis of symmetry (*Blankenship and Bentley, 1987*). This is due to crystal-orientation fabrics (COFs), where crystal orientations are commonly referenced to the *c*-axis, which is perpendicular to the basal plane, or the distribution of *c*-axes on a lower-hemisphere Schmidt projection (*Bennett, 1968; Blankenship and Bentley, 1987*). Typically, ice-divide observations show nearly randomly distributed *c*-axis orientations in the near surface. With increasing depth, the *c*-axes rotate towards the vertical direction due to vertical compression or simple shear. In the late 1950s and early 1960s, some researchers started to note the presence of weak englacial seismic reflections (e.g. *Bentley and Osteno, 1961*) a few hundred meters above the bedrock, with an amplitude of approximately one tenth that of the bedrock reflection (*Bentley, 1971*). These reflections are detected as continuous bed-conformable englacial reflectivity. All the subsequent seismic studies have attributed englacial reflectivity to either entrained basal-material or abrupt changes in COF (*Smith, 1996; Anandakrishnan, 1996; Horgan et al., 2008; Horgan et al., 2011*). Another interpretation of this phenomenon can be the presence of fractures favoured by the proximity of the bedrock, in particular if the basal topography is pronounced.

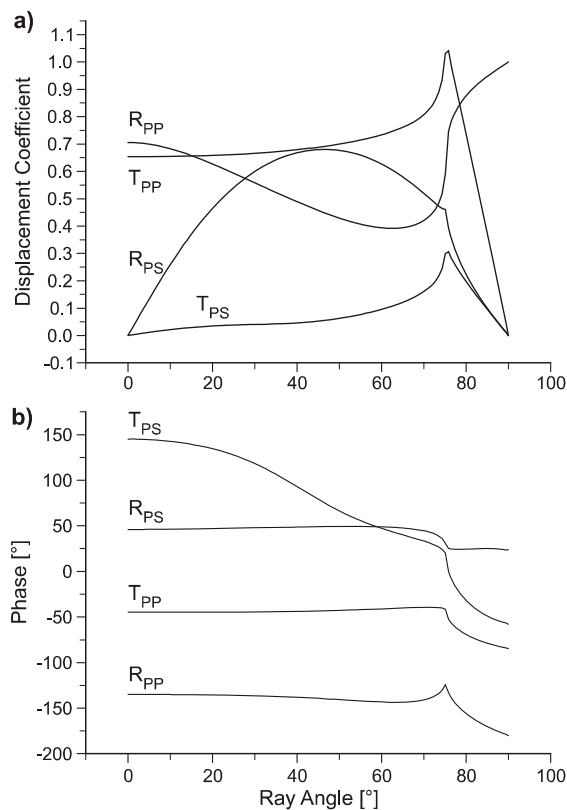


**Fig. 2.** a) Modulus and b) phase of the displacement coefficients as a function of the ray angle for  $f = 100$  Hz.

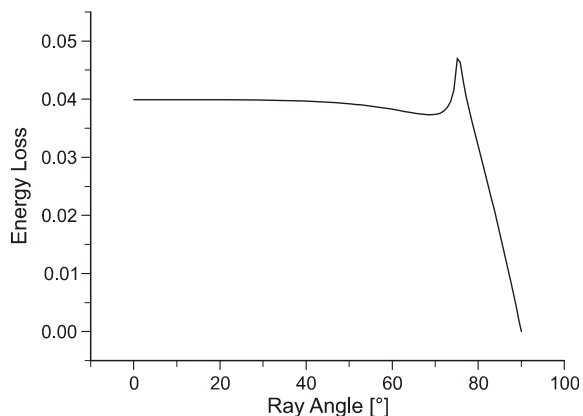


**Fig. 3.** Energy loss as a function of the ray angle for  $f = 100$  Hz.

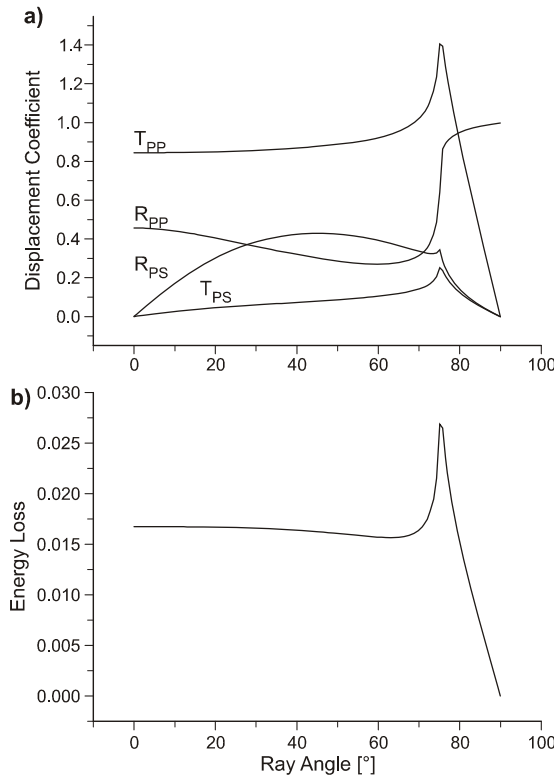


**Fig. 4.** a) Modulus of the displacement coefficients and b) energy loss as a function of the ray angle for  $f = 50$  Hz.

We consider a planar fracture at 2.6 km depth in the ice sheet. The ice sheet at that depth has the properties

$$c_{11} = 16 \text{ GPa}, \quad c_{13} = 6.5 \text{ GPa}, \quad c_{33} = 14 \text{ GPa}, \quad c_{55} = 3 \text{ GPa}, \quad \rho = 920 \text{ kg/m}^3 \quad (35)$$

and

$$c_{11} = 18 \text{ GPa}, \quad c_{13} = 6.5 \text{ GPa}, \quad c_{33} = 16 \text{ GPa}, \quad c_{55} = 4 \text{ GPa}, \quad \rho = 940 \text{ kg/m}^3 \quad (36)$$

above and below the fracture, respectively (e.g., *Carcione and Gei, 2003*). See *Thiel and Osteno (1961)* and *Blankenship and Bentley (1987)* for more information about the elasticity constants of the ice cap.

The fracture has the following parameters:  $\kappa_x = \pi f_0 I_S$ ,  $\kappa_z = \pi f_0 I_P$ ,  $\eta_x = I_S / 50$  and  $\eta_z = I_P / 50$ , where  $f_0 = 100$  Hz is a reference frequency and  $I_S = \sqrt{\rho c_{55}}$ . The compliances values are  $1/\kappa_x = 1.9 \times 10^{-9} \text{ m/Pa}$  and  $1/\kappa_z = 8.9 \times 10^{-10} \text{ m/Pa}$ , which are in agreement with values used in the literature (*Chaisri and Krebes, 2000; Nakagawa and*

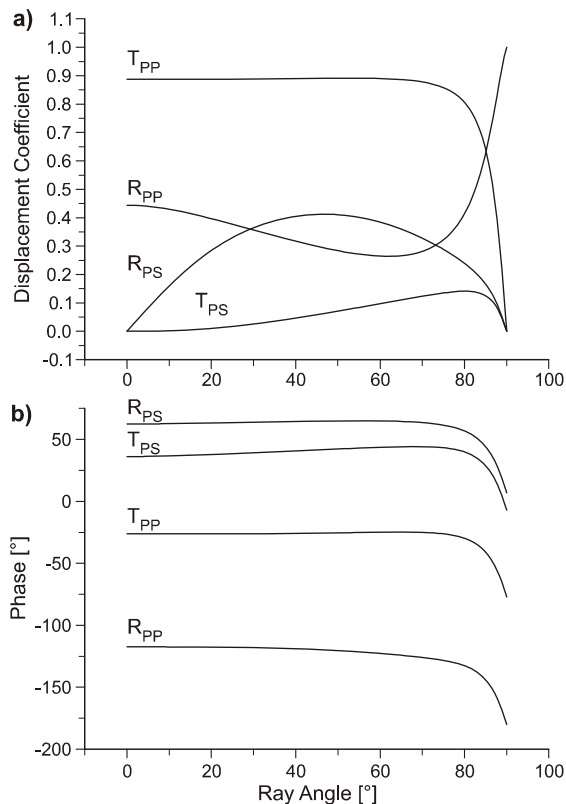


**Fig. 5.** a) Modulus and b) phase of the displacement coefficients as a function of the ray angle for  $f = 50$  Hz. The medium is homogeneous (the upper and lower media are the same).

Myer, 2009). The complex compliances (23) represent viscoelastic Kelvin-Voigt models (Carcione, 1996, 2007) and a quality factor can be defined as  $Q_i = \kappa_i / (\omega \eta_i)$ . In this case,  $Q = 25f_0/f$ , where  $f = \omega/(2\pi)$ , which can be useful to quantify the energy loss at the fracture. Fig. 2a shows the modulus and Fig. 2b the phase of the displacement coefficients as a function of the ray angle for  $f = 100$  Hz ( $Q_i = 25$ ), and Fig. 3 shows the energy loss, indicating that 4% of the energy is lost at the fracture at  $\psi = 0$ . The amplitude peaks at nearly  $75^\circ$  due to PP critical-angle, where maximum attenuation occurs. The modulus of the reflection and transmission displacement coefficients for  $f = 50$  Hz are displayed in Fig. 4a and energy loss in Fig. 4b. In this case  $Q_i = 50$ , implying less energy dissipation (1.6%). The reflection coefficient is lower than in the previous case, where  $f = 100$  Hz. Thus, the fracture acts as a low-pass filter for the transmitted P wave. In the absence of fracture ( $\kappa_i \rightarrow \infty$ ,  $\eta_i \rightarrow \infty$  or  $c_x = c_z = 0$ ), the PP reflection coefficient is small at near and moderate angles (less than 0.04).

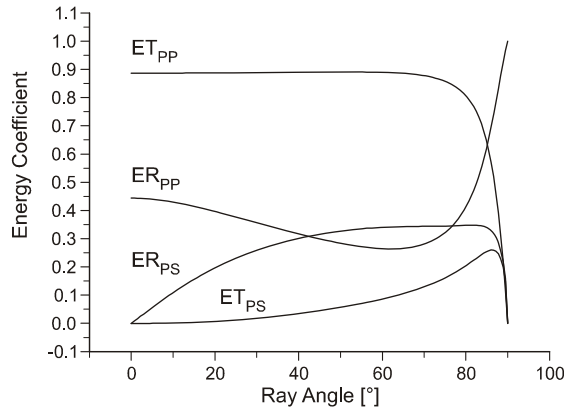


**Fig. 6.** Energy coefficients as a function of the ray angle for  $f = 50$  Hz. The medium is homogeneous (the upper and lower media are the same).

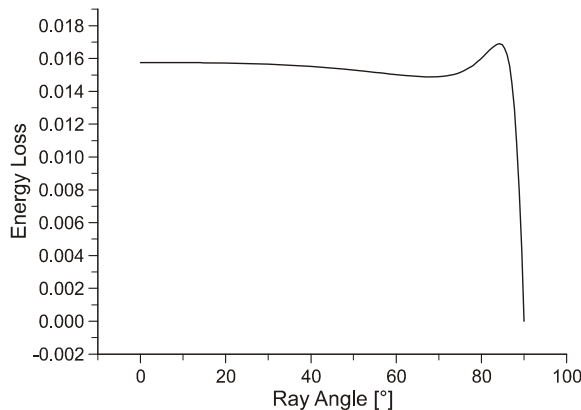


**Fig. 7.** Energy loss as a function of the ray angle for  $f = 50$  Hz. The medium is homogeneous (the upper and lower media are the same).

Fig. 5 shows the displacement coefficients, Fig. 6 the energy coefficients and Fig. 7 the energy loss for  $f = 50$  Hz and an homogeneous medium, whose properties are those of the upper medium. The critical-angle effect has disappeared. The dependence with frequency is displayed in Fig. 8, where it can be seen that the reflection coefficient and dissipated energy decrease with decreasing frequency, confirming the low-pass filter property mentioned above. If  $\omega \rightarrow \infty$  the energy loss (33) approaches the limiting value  $4(\eta_z/I_P)/(1+2\eta_z/I_P)^2$ .

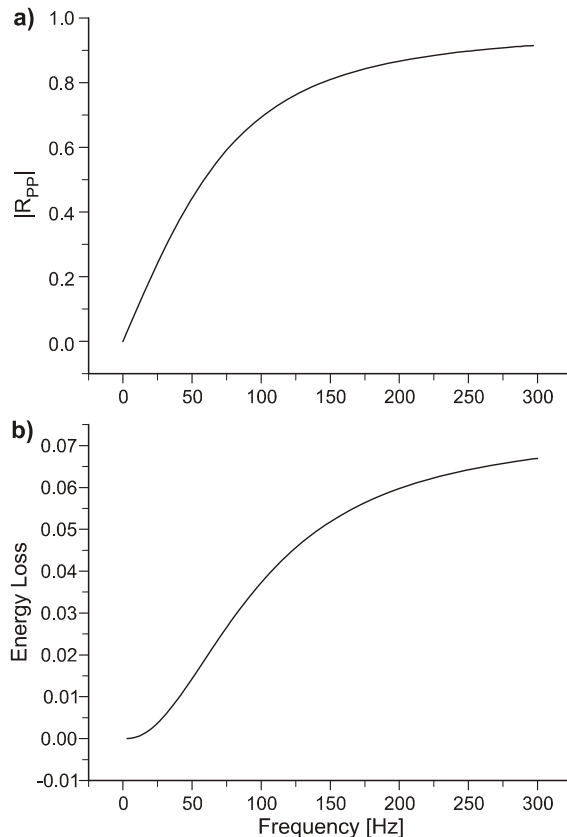


**Fig. 8.** a) Normal incidence PP reflection displacement coefficient and b) energy loss as a function of frequency. The medium is homogeneous (the upper and lower media are the same).

## 7. CONCLUSIONS

A general linear model of an imperfect interface (e.g., a fracture) between two elastic media can be obtained by imposing boundary discontinuities to the displacement and particle-velocity fields. The model can be expressed as displacement and particle-velocity discontinuities equivalent to a viscoelastic model. The P-S wave propagation problem requires two specific stiffnesses and two specific viscosities, which define the properties of the non-ideal contact. Different choices of fracture parameters give rise to the different conditions, from welded contact to stress-free boundary condition. The proposed model yields the reflection and transmission coefficients of a fracture embedded in transversely isotropic media. The fracture surface dissipates energy due to attenuation mechanisms present at the fracture, as for instance, the interaction between a viscous fluid with the solid media. The fracture acts as a low-pass filter for the transmitted P wave and the reflection coefficient decreases at small and moderate ray angles.

*Acknowledgments:* We thank Ivan Pšenčík for useful comments.

*References*

- Aki K. and Richards P.G., 1980. *Quantitative Seismology: Theory and Methods*. W.H. Freeman and Co., San Francisco, CA.
- Anandakrishnan S., 1996. Seismic reflections from an internal layer: Fabric change or moraine? *Eos Trans. AGU*, **77**.
- Backus G.E., 1962. Long-wave elastic anisotropy produced by horizontal layering. *J. Geophys. Res.*, **67**, 4427–4440.
- Bennett H.F., 1968. *An Investigation into Velocity Anisotropy through Measurements of Ultrasonic-Wave Velocities in Snow and Ice Cores from Greenland and Antarctica*. PhD Thesis. University of Wisconsin, Madison.
- Bentley C.R. and Osteno N.A., 1961. Glacial and subglacial topography of West Antarctica. *J. Glaciol.*, **3**, 882–911.
- Bentley C.R., 1971. Seismic evidence for moraine within the basal Antarctic ice sheet. In: Crary A.P. (Ed.), *Antarctic Snow and Ice Studies II*. Antarctic Research Series, **16**, American Geophysical Union, Washington, D.C.
- Barton N., 2007. Fracture-induced seismic anisotropy when shearing is involved in production from fractured reservoirs. *J. Seism. Explor.*, **16**, 115–143.
- Blankenship D.D. and Bentley C.R., 1987. The crystalline fabric of polar ice sheets inferred from seismic anisotropy. In: Waddington E.D. and Walder J.S. (Eds.), *The Physical Basis of Ice Sheet Modelling*. IAHS Publ. No. 170 ([http://iahs.info/redbooks/a170/iahs\\_170\\_0017.pdf](http://iahs.info/redbooks/a170/iahs_170_0017.pdf)).
- Carcione J.M., 1996. Elastodynamics of a non-ideal interface: Application to crack and fracture scattering. *J. Geophys. Res.*, **101**, 28177–28188.
- Carcione J.M., 1997. Reflection and transmission of qP-qS plane waves at a plane boundary between viscoelastic transversely isotropic media. *Geophys. J. Int.*, **129**, 669–680.
- Carcione J.M., 1998. Scattering of elastic waves by a plane crack of finite width in a transversely isotropic medium. *Int. J. Numer. Anal. Methods Geomech.*, **22**, 263–275.
- Carcione J.M., 2007 (Ed.). *Wave Fields in Real Media: Wave Propagation in Anisotropic, Anelastic, Porous and Electromagnetic Media*. 2nd Edition, Handbook of Geophysical Exploration, **38**, Elsevier, Amsterdam, The Netherlands.
- Carcione J.M. and Gei D., 2003. A seismic modeling study of a subglacial lake. *Geophys. Prospect.*, **51**, 501–515.
- Chaisri S. and Krebes E.S., 2000. Exact and approximate formulas for P-SV reflection and transmission coefficients for a nonwelded contact interface. *J. Geophys. Res.*, **105**, 28045–28054.
- Coates R.T. and Schoenberg M., 1995. Finite-difference modelling of faults and fractures. *Geophysics*, **60**, 1514–1526.
- Fan L.F., Ren F. and Ma G.W., 2011. An extended displacement discontinuity method for analysis of stress wave propagation in viscoelastic rock mass. *J. Rock Mech. Geotech. Eng.*, **3**, 73–81.

- Grechka V. and Tsvankin I., 2003. Feasibility of seismic characterization of multiple fracture sets. *Geophysics*, **68**, 1399–1407.
- Hall S.A. and Kendall J.M., 2003. Fracture characterization at Valhall: Application of P-wave amplitude variation with off set and azimuth AVOA analysis to a 3D oceanbottom data set. *Geophysics*, **68**, 1150–1160.
- Hansen B.R.H., 2002. *Evaluating the Impact of Fracture-Induced Anisotropy on Reservoir Rock Property Estimates Made from Seismic Data*. Report No.GPH 7/02, Curtin University of Technology, Perth, Australia.
- Horgan H.J., Anandakrishnan S., Alley R.B., Burkett P.G. and Peters L.E., 2011. Englacial seismic reflectivity: Imaging crystal orientation fabric in West Antarctica. *J. Glaciol.*, **57**, 639–650.
- Horgan H.J., Anandakrishnan S., Alley R.B., Peters L.E., Tsolfias G.P., Voigt D.E. and Winberry J.P., 2008. Complex fabric development revealed by englacial seismic reflectivity: Jakobshavn Isbrae, Greenland. *Geophys. Res. Lett.*, **35**, L10501.
- Kundu T. and Boström A., 1992. Elastic wave scattering by a circular crack in a transversely isotropic solid. *Wave Motion*, **15**, 285–300.
- Mroz Z. and Giambianco G., 1996. An interface model for analysis of deformation behaviour of discontinuities. *Int. J. Num. Anal. Methods Geomech.*, **20**, 1–33.
- Nagy P.B. and Adler L., 1990. New ultrasonic techniques to evaluate interfaces. In: Datta S.K., Achenbach J.D. and Rajapakse Y.S. (Eds.), *Elastic Waves and Ultrasonic Nondestructive Evaluations*. North-Holland, Amsterdam, The Netherlands, 229–239.
- Nakagawa S. and Myer L.R., 2009. Fracture permeability and seismic wave scattering - poroelastic linear-slip interface model for heterogeneous fractures. *SEG Expanded Abstracts*, **28**, 3461, DOI: 10.1190/1.3255581.
- Perino A., Zhu J.B., Li J.C., Barla G. and Zhao J., 2010. Theoretical methods for wave propagation across jointed rock masses. *Rock Mech. Rock Eng.*, **43**, 799–809.
- Pyrak-Nolte L.J., Myer L.R. and Cook N.G.W., 1990. Transmission of seismic waves across single natural fractures. *J. Geophys. Res.*, **95**, 8617–8638.